Molecular Engineering of C₆₀-Based Conjugated Oligomer Ensembles: Modulating the Competition between Photoinduced Energy and Electron Transfer Processes

Dirk M. Guldi,* Chuping Luo, and Angela Swartz

Radiation Laboratory, University of Notre Dame, Indiana 46556

Rafael Gómez, José L. Segura, and Nazario Martín*

Departamento de Química Orgánica, Facultad de Química, Universidad Complutense,
E-28040 Madrid, Spain

Christoph Brabec and N. Serdar Sariciftci*

Christian Doppler Laboratory for Plastic Solar Cells, Linz Institute for Organic Solar Cells (LIOS),
Physical Chemistry, Johannes Kepler University Linz, A-4040 Linz, Austria

nazmar@quim.ucm.es

A series of novel and soluble C_{60}−(π-conjugated oligomer) dyads were synthesized, starting from suitably functionalized oligomer precursors (i.e., dihexyloxynaphthalene, dihexyloxynaphthalene−thiophene, and dihexyloxybenzene−thiophene). A systematic change in the nature of the oligomeric component allowed (i) tailoring the light absorption of the chromophore by shifting the ground-state absorption from the ultraviolet to the visible region and (ii) varying the oxidation potential of the donor. The resulting electro- and photoactive dyads were examined by electrochemical and photophysical means. In general, both singlet−singlet energy transfer and intramolecular electron transfer were found to take place and, most importantly, to compete with each other in the overall deactivation of the photoexcited oligomer. The selection of polar solvents in combination with the dihexyloxybenzene−thiophene donor shifted the reactivity from an all energy (**1a**; dihexyloxynaphthalene) to an all electron-transfer scenario (**1d**, dihexyloxybenzene−thiophene). Encouraged by the favorable electron-transfer properties of dyad **1d,** we prepared photodiodes by embedding **1d** between asymmetric metal contacts, which showed external monochromatic efficiencies (IPCE) close to 10% at the maximum absorption of the molecule.

Introduction

Oligomeric architectures have assumed paramount importance as a diverse platform for conducting systematic chemistry. Importantly, owing to the wide-range significance of these low-molecular mass building blocks, considerable attention has focused on employing them as references for their larger and more complex polymeric analogues.[1] Major efforts have been invested into their examinations, for example, as model systems to (i) clarify the relationships between substitution pattern, solid-state structure and emission properties and other electrooptical properties of conjugated materials,[2] (ii) apply quantum-chemical approaches to the determination of optical phenomena and transport properties,[3] (iii) rationalize the electrochemical behavior,[4] and (iv) investigate the photophysical properties of conjugated polymers.[5] In many aspects, well-defined monodisperse oligomers have now advanced into strong fields on their own.[6,7]

Current trends in polymer chemistry/physics are rapidly moving toward smaller devices with high integration densities. This development, that is, shifting from micro- to nanoelectronics, implies molecular electronics/photonics that exhibit full functionality on the smallest realizable scale. Guided by the concepts of semiconductor technology, the design of molecules with electronic/photonic functions is one viable route toward organic photovoltaic applications[8−10] and molecular electronics.[11−15]

(1) Van Hutten, P. F.; Krasnikov, V. V.; Hadziioannou, G. *Acc. Chem. Res.* **1999,** *32,* 257.

(2) Garnier, F. *Acc. Chem. Res.* **1999,** *32,* 209.

(3) (a) Brédas, J. L. *Adv. Mater.* **1995,** *7,* 263. (b) Brédas, J. L.; Cornil, J.; Beljonne, D.; Dos Santos, D. A.; Shuai, Z. *Acc. Chem. Res.* **1999,** *32,* 267.

(4) Heinze, J.; Tschuncky P. *Electronic materials: the oligomer approach*; Müllen, K., Wegner, G., Eds.; Wiley-VCH: Weinheim, 1998; pp 479−513.

(5) Bässler, H.; Schweitzer, B. *Acc. Chem. Res.* **1999,** *32,* 173.

(6) Segura, J. L.; Martín, N. *J. Mater. Chem.* **2000,** *10,* 2403.

(7) Martín, R. E.; Diederich, F. *Angew. Chem., Int. Ed.* **1999,** *38,* 1350.

(8) (a) Sariciftci, N. S.; Smilowitz, L.; Heeger, A. J.; Wudl, F. *Science* **1992,** *258,* 1474. (b) Sariciftci, N. S. *Prog. Quantum Electron.* **1995,** *19,* 131. (c) Sariciftci, N. S.; Heeger, A. J. In *Handbook of Organic Conductive Molecules and Polymers*; Nalwa, H. S., Ed.; Wiley: New York, 1996. (c) Brabec, C. J.; Sariciftci, N. S.; Hummelen, J. C. *Adv. Funct. Mater.* **2001,** *11,* 15.

(9) Yu, G.; Gao, Y.; Hummelen, J. C.; Wudl, F.; Heeger, A. J. *Science* **1995,** *270,* 1789.

(10) (a) Granström, M.; Petritsch, K.; Arias, A. C.; Lux, A.; Andersson, M. R.; Friend, M. R. *Nature* **1998,** *395,* 257. (b) Gao, J.; Yu, G.; Heeger, A. J. *Adv. Mater.* **1998,** *10,* 692. (c) van Hal, P. A.; Christiaans, M. P. T.; Wienk, M. M.; Kroon, J. M.; Janssen, R. A. J. *J. Phys. Chem. B* **1999,** *103,* 4352. (d) Huynh, W. U.; Peng, X.; Alivisatos, A. P. *Adv. Mater.* **1999,** *11,* 923. (e) Halls, J. J. M.; Arias, A. C.; Mackenzie, J. D.; Wu, W.; Inbasekaran, M.; Woo, E. P.; Friend, R. H. *Adv. Mater.* **2000,** *12,* 498. (f) Wallace, G. G.; Dastoor, P. C.; Officer, D. L.; Too, C. O. *Chem. Innovation* **2000,** *30*(1), 14.

(11) Carter, F. L. *Molecular Electronic Devices*; Marcel Dekker: New York, 1987; Vol. II.

As far as the performance of organic photovoltaic devices (i.e., a conjugated polymer/fullerene blend) is concerned, the overriding principle is an intermolecular electron transfer from the photoexcited polymer to the electron accepting fullerene. A major shortcoming is the tendency, especially that of pristine C_{60}, to phase-separate and subsequently to crystallize. This imposes important limitations on the solubility of C_{60} within a conjugated polymer matrix.

Uniformity and high quality of conjugated polymer/fullerene thin films are, however, essential requisites for device fabrication. Thus, different synthetic strategies have been refined to overcome the problem of phase separation. In the earlier years, the design of soluble fullerene derivatives was pursued to secure control over the morphology of the interpenetrating networks: Homogeneous and stable blends, containing more than 80 wt % fullerenes were manufactured by using functionalized fullerene derivatives rather than pristine fullerene materials.[10] Succeeding this area, conjugated-polymer structures, bearing covalently linked fullerene moieties (i.e., in-chain versus on-chain), of different complexity emerged as viable alternatives for fabricating stable bicontinuous networks. More recently, the benefits of monodisperse conjugated-oligomers, eminently easier to handle and to characterize, have been acclaimed through the development of $C_{60}-(\pi$-conjugated oligomer) donor−acceptor arrays.

In recognition of this importance, several donor−acceptor arrays[16,17] (i.e., π-conjugated oligomer/fullerene) have been probed in time-resolved and steady-state photolytic experiments. One of the most striking features of $C_{60}-(\pi$-conjugated oligomer) systems is that their excited-state dynamics are dominated by a competition between rapid energy and electron-transfer reactions. The outcome of this contest depends largely on the nature of the π-conjugated oligomeric system, as well as on the number of repeating units in the oligomer. Importantly, contributions stemming from an energy transfer lower the photovoltaic conversion efficiency.

To understand better the relationship between electron and energy transfer in $C_{60}-(\pi$-conjugated oligomer) ensembles, we have developed several new synthetic model systems (**1a−d**). In particular, different arylene units ranging from naphthalene and benzene to thiophene have been incorporated into a π-conjugated backbone as singlet excited-state electron donors. A covalent linkage juxtaposes these donors to a fullerene moiety as the acceptor. With these new building blocks, the ground-state as well as the excited-state properties of the resulting electroactive dyads were systematically fine-tuned. The incentives are 3-fold: First, to impact the overall thermodynamics (i.e., facilitate or retard intramolecular electron-transfer processes); second, to influence the competition between the dominant singlet−singlet energy transfer and electron-transfer events (i.e., shifting the deactivation of the photoexcited chromophore from an energy to an electron-transfer scenario); and third, to exploit the photovoltaic properties of these new donor−acceptor structures.

Results and Discussion

Synthesis. Among the suitable protocols for the functionalization of fullerenes, the 1,3-dipolar cycloaddition of azomethine ylides to C_{60} is an important methodology for the production of stable fullerene derivatives.[18] To date, a broad spectrum of intriguing fulleropyrrolidine derivatives, bearing electro- and/or photoactive addends, have been synthesized via this procedure.[19] Therefore, we targeted at the synthesis of conjugated oligomers with an aldehyde group, enabling us to adapt this synthetic methodology for the production of $C_{60}-(\pi$-conjugated oligomer) dyads.

Scheme 1 summarizes the synthetic pathways and reaction conditions, which were selected en route to the required conjugated systems. Specifically, Wittig reaction of aldehydes **3b**[20] and commercially available **8b** with bis-[(triphenylphosphonium)methyl]naphthalene **2**[20] and bis-[(triphenylphosphonium)methyl]benzene **14**[21a] afforded the corresponding dibromosubstituted compounds **5**,[20] **10**,[21b] and **16**.

As the reaction of semistabilized triphenylphosphonium benzylides with aldehydes affords mixtures of (*Z*)- and (*E*)-alkenes nonstereospecifically,[22] **5**, **10**, and **16** were obtained as mixtures of trans−trans isomers enriched with the corresponding cis−trans and cis−cis analogues. This required isomerization of the reaction mixture to the all-trans isomers via reflux in xylene, containing a catalytic trace of iodine. The enhanced solubility of these compounds, stemming mainly from the flexible side chains, allowed monitoring of this aspect by high-resolution NMR. In particular, a ^3J value of 16 Hz of the vinylic protons relates to the trans-trans configuration. Moreover, the ^{1}H NMR spectra recorded after completion of the isomerization reaction is much simpler than that of the starting isomeric mixture. A similar simplification of the ^{13}C NMR spectra was observed after isomerization.

The Rosenmund von Braun reaction[23] of the dibromo derivatives **5**, **10**, and **16**, namely, the treatment with copper cyanide in dry *N,N*-dimethylformamide in the presence of a catalytic amount of sodium iodide, yielded

(12) Carter, F. L.; Siatkowski, R. E.; Wohltjen, H. *Molecular Electronic Devices*; North-Holland: Amsterdam, 1988.

(13) Aviram, A. *Molecular Electronics−Science and Technology*; United Engineering Trustees: New York, 1989.

(14) Hong, F. T. *Molecular Electronics−Biosensors and Biocomputers*; Plenum Press: New York, 1989.

(15) Jortner, J.; Ratner, M. In *Molecular Electronics*; Blackwell Science Ltd: Oxford, 1997.

(16) Segura, J. L.; Gómez, R.; Martín, N.; Luo, C.; Guldi, D. M. *Chem. Commun.* **2000**, 701.

(17) (a) Nierengarten, J.-F.; Eckert, J.-F.; Nicoud, J.-F.; Ouali, L.; Krasnikov, V.; Hadziioannou, G. *Chem. Commun.* **1999**, 617. (b) Eckert, J.-F.; Nicoud, J.-F.; Nierengarten, J.-F.; Liu, S. G.; Armaroli, N.; Ouali, L.; Krasnikov, V.; Hadziioannou, G. *J. Am. Chem. Soc.* **2000**, *122*, 7467. (c) Armaroli, N.; Barigelleti, F.; Ceroni, P.; Eckert, J.-F.; Nicoud, J.-F.; Nierengarten, J.-F. *Chem. Commun.* **2000**, 599. (d) Yamashiro, T.; Aso, Y.; Otsubo, T.; Tang, H.; Harima, Y.; Yamashita, K. *Chem. Lett.* **1999**, 443. (e) Knorr, S.; Grupp, A.; Mehring, M.; Grube, G.; Effenberger, F. *J. Chem. Phys.* **1999**, *110*, 3502. (f) Peeters, E.; van Hal, P. A.; Knol, J.; Brabec, C. J.; Sariciftci, N. S.; Hummelen, J. C.; Janssen, R. A. J. *J. Phys. Chem. B* **2000**, *104*, 10174. (g) Martini, I.; Ma, B.; da Ros, T.; Helgeson, R.; Wudl, F.; Schwartz B. *J. Chem. Phys. Lett.* **2000**, *327*, 253.

(18) Prato, M.; Maggini, M. *Acc. Chem. Res.* **1998**, *31*, 519.

(19) (a) Martín, N.; Sánchez, L.; Illescas, B.; Pérez, I. *Chem. Rev.* **1998**, *98*, 2527. (b) Imahori, H.; Sakata, Y. *Adv. Mater.* **1997**, *9*, 537. (c) Imahori, H.; Sakata, Y. *Eur. J. Org. Chem.* **1999**, 2445.

(20) Segura, J. L.; Martín, N.; Hanack, M. *Eur. J. Org. Chem.* **1999**, 643.

(21) (a) Pang, Y.; Li, J.; Hu, B.; Karasz, E. *Macromolecules* **1999**, *32*, 3946. (b) Gómez, R.; Segura, J. L.; Martín, N. *J. Org. Chem.* **2000**, *65*, 7501.

(22) (a) Johnson, A. W. *Ylides and Imines of Phosphorous*; John Wiley & Sons: New York, 1993; Chapters 3 and 9. (b) Wennerström, O.; Raston, J.; Sundahl, M.; Tanner, D. *Chem. Scr.* **1987**, *27*, 567.

(23) Ellis, G. P.; Romney-Alexander, T. M. *Chem. Rev.* **1987**, *87*, 779.

Scheme 1
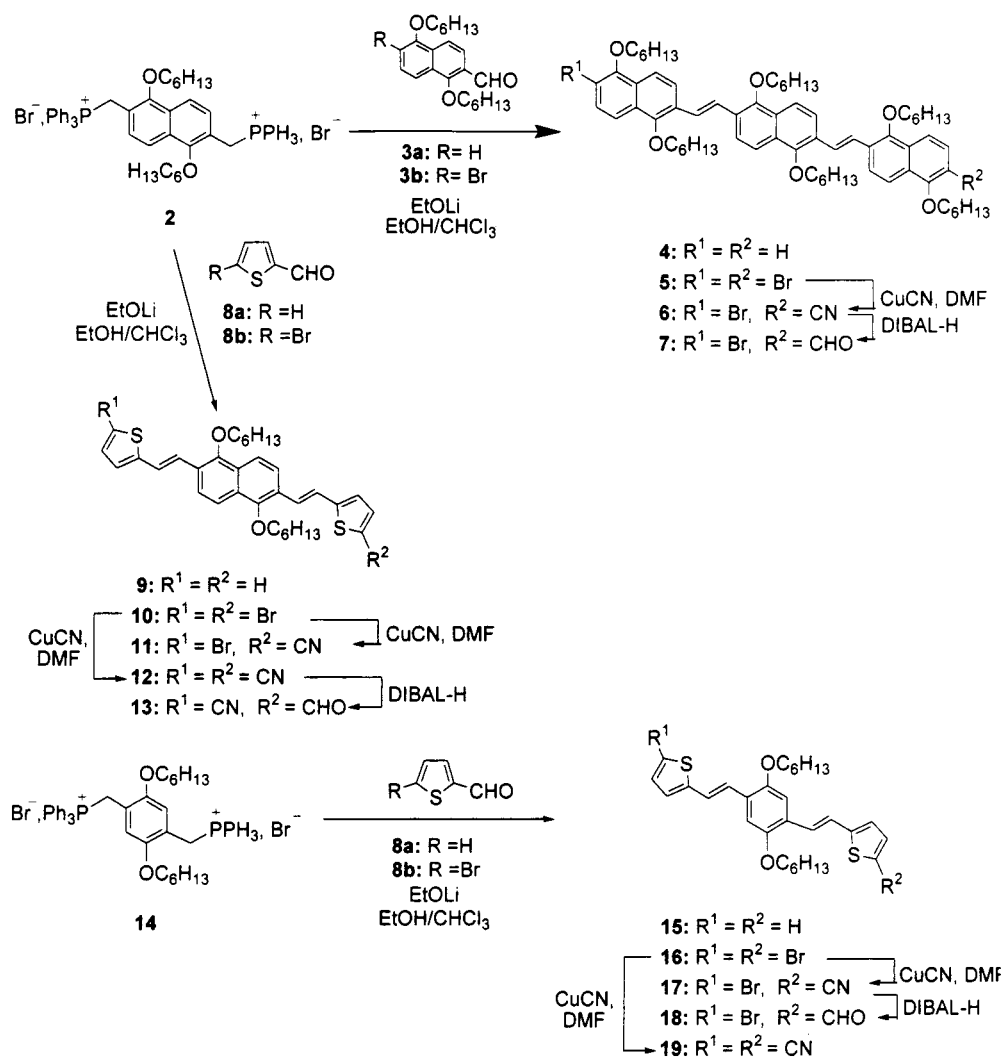
a mixture of the monocyano (**6**, **11**, and **17**) and dicyano derivatives (**12** and **19**). These were subsequently separated by column chromatography. Selective reduction of the nitrile groups using diisobutylaluminum hydride[24] yielded monaldehydes **7**, **13**, and **18** almost quantitatively. Although the direct formylation of the bromoderivatives, by using the Bouveault method,[25] was also employed, the two-step reaction sequence involving the Rosenmund von Braun reaction, followed by treatment with DIBAL-H (see Scheme 1), proved to be more efficient. Two factors are responsible for this trend: (i) the global yield was higher and (ii) the cyano derivatives were easier to separate than the aldehydes.

Unsubstituted π-conjugated systems **4**,[20] **9**, and **15**, which are reference compounds for the electrochemical and photophysical studies, were synthesized by a similar Wittig reaction involving the bis(triphenylphosphonium) salts **2** and **14**, formylnaphthalene **3a**,[20] and formylthiophene **8a**, respectively (Scheme 1). Iodine-catalyzed thermal isomerization was also deemed necessary to obtain pure all-trans isomers.

The monoaldehydes **7**, **13**, and **18** were selected as starting materials for the preparation of dyads **1a−d**, in addition to 2-bromo-6-formyl-1,5-dihexyloxynaphthalene (**3b**),[20] which was employed in the synthesis of dyad **1a**. Treating monoaldehydes **3b**, **7**, **13**, and **18** with C$_{60}$ and excess sarcosine in refluxing toluene for 24 h yielded dyads **1a−d** (Scheme 2). Due to the presence of the long alkoxy substituents, these dyads are highly soluble in common organic solvents, and complete spectroscopic characterization was achieved.

In CDCl$_3$ solutions, the ^{1}H NMR spectra of the compounds investigated reveal that the stereochemistry of the vinylenic double bonds remains unaffected after the cycloaddition reaction. The fulleropyrrolidine signals appear, for instance, at around 5.1 ppm (CH) as a singlet and a set of two doublets (CH$_2$) with coupling constants around $J = 9.8$ Hz, integrating for one hydrogen. On the other hand, the ^{13}C NMR spectra show the signals originating from the conjugated oligomer moiety as well as from the fullerene system. Specifically, in addition to the characteristic fullerene's sp^2 region another four signals, which correspond to the sp^3 carbon atoms of the fulleropyrrolidine ring, were noted between 70 and 80 ppm and further complemented by those of the hexyloxy chains between 70 and 15 ppm.

Electrochemistry. The electrochemical features of dyads **1a−d** were probed by cyclic voltammetry at room temperature. The redox potentials are collected in Table

(24) Marshall, J. A.; Andersen, W. H.; Schrider, J. W. *J. Org. Chem.* **1970**, *35*, 858.

(25) Meiler, D.; Semmelhack, M. F. *Org. Synth.* **1986**, *64*, 114.

Scheme 2
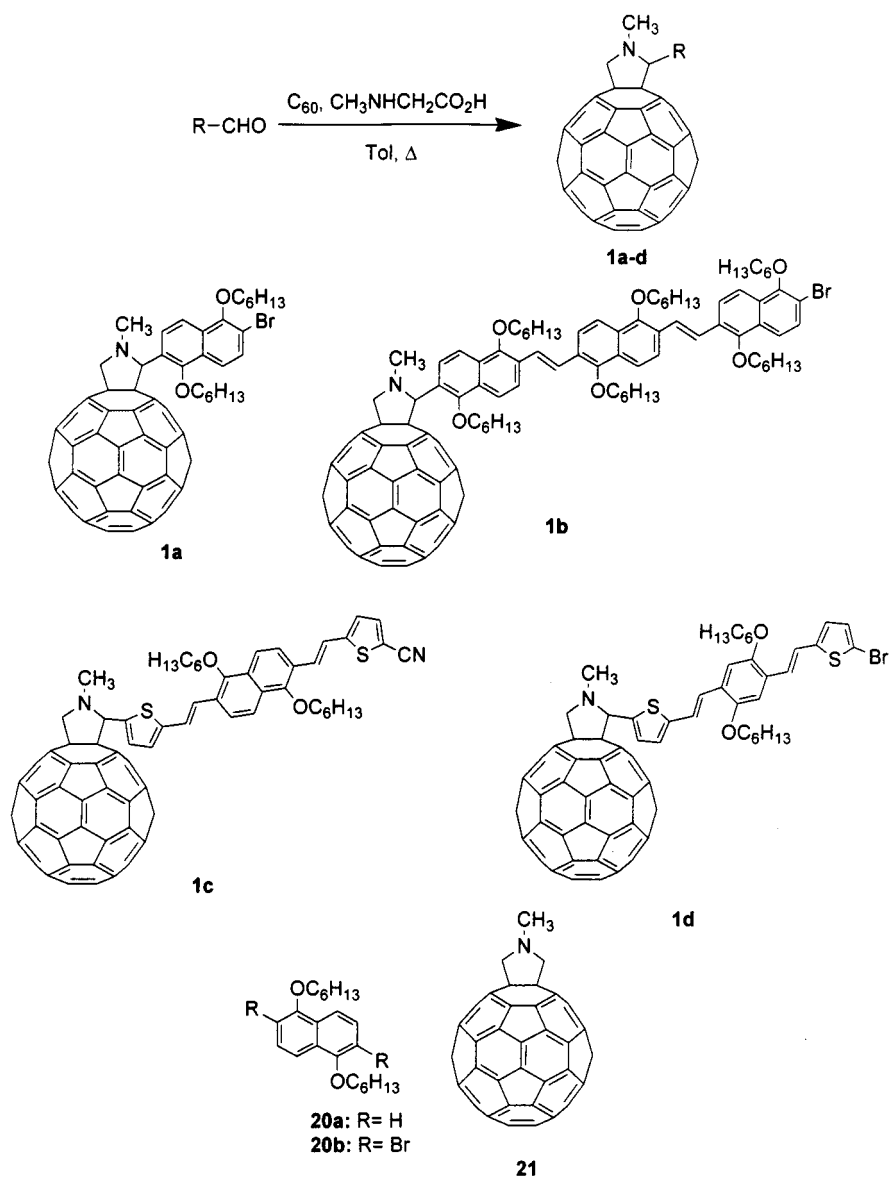
Table 1. Redox Potentials and UV–Vis Maxima of Fullerene-Based Dyads 1 and Reference Compounds

compd	$E^1_{pa}{}^a$	$E^1_{pc}{}^b$	E^2_{pc}	E^3_{pc}	E^4_{pc}	λ_{max} (nm)
20a	1.41					328
1a	1.49	−0.62	−1.09	−1.62		328
4	1.31					413
1b	1.44	−0.66	−1.04	−1.66		422
9	1.20					412
1c	1.30	−0.65	−1.02	−1.69	−1.94	432
15	1.01					412
1d	1.08	−0.65	−1.07	−1.64		422
21	1.32	−0.71	−1.14	−1.75		322

^{a} pa: anodic peak. ^{b} pc: cathodic peak. In dichloromethane solutions using Bu$_4$NClO$_4$ (0.3 mg L^{-1}, SCE reference electrode and glassy carbon as working electrode).

1 and compared with those of the unsubstituted π-conjugated (**4**, **9**, **15**, and **20**[20]) and fulleropyrrolidine (**21**) references.[26]

As a general feature, dyads **1a**−**d** give rise to three quasireversible one-electron reduction waves that reflect the first three one-electron reduction steps of the fullerene cores. These reduction potential values are shifted to more negative values relative to that of pristine [60]-fullerene. The underlying cathodic shift stems from the saturation of a double bond of the C$_{60}$ core, which, accordingly, raises the lowest unoccupied molecular orbital (LUMO) energy of the resulting fullerene derivative.[27] A closer inspection of the data reveals that the first reduction potential values of these dyads are all similar. Furthermore, they compare quite well with that of the fulleropyrrolidine reference (see Figure S1).

The redox behavior of the conjugated π-systems shows an increase of the donor strength, when going from dihexyloxynaphthalene (**20a**: $E_{ox} = 1.41$ V) to the trimeric analogue (**4**: $E_{ox} = 1.31$ V), and also upon replacing the peripheral naphthalene units in the trimer by the π-excedent thiophene ring (**9**: $E_{ox} = 1.20$ V). The best

(26) Williams, R. M.; Zwier, J. M.; Verhoeven, J. W. *J. Am. Chem. Soc.* **1995**, *117*, 4093.

(27) (a) Suzuki, T.; Maruyama, T.; Akasaba, T.; Ando, W.; Kobayashi, K.; Nagase, S. *J. Am. Chem. Soc.* **1994**, *116*, 1359. (b) Chlistouff, J.; Cliffel, D.; Bard, A. J. In *Handbook of Organic Conductive Molecules and Polymers*; Nalwa, N. S., Ed.; John Wiley & Sons: New York, 1997; Vol. 1, Chapter 7. (c) Echegoyen, L.; Echegoyen, L. E. *Acc. Chem. Res.* **1998**, *31*, 593.
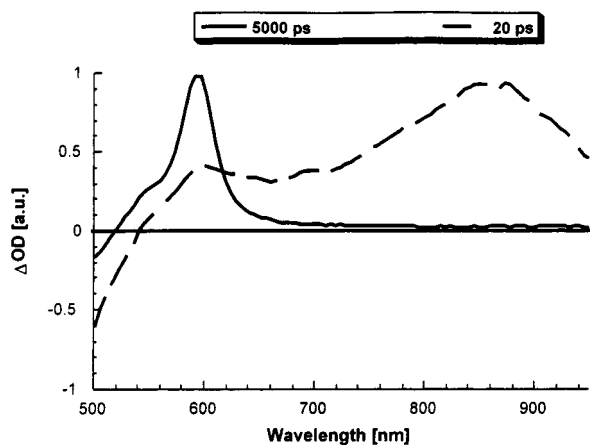
Figure 1. Transient absorption spectrum (visible-near-infrared part) recorded 20 ps (dashed line) and 5000 ps (solid line) upon flash photolysis of reference **9** (2.0×10^{-5} M) at 355 nm in deoxygenated toluene, indicating the oligomer singlet–singlet ($\lambda_{max} = 850$ nm) and triplet–triplet features ($\lambda_{max} = 580$ nm), respectively.

results, in terms of oxidation, were observed for the π-conjugated system, in which the central naphthalene moiety is replaced by a phenylene unit (**15**: $E_{ox} = 1.01$ V). This trend is in good agreement with previous studies on conjugated oligomers containing naphthalene, thiophene, and phenylene units.[26,28] Interestingly, the presence of the large naphthalene system induces some steric interactions that presumably lead to a decrease in the conjugation of these systems. In turn, this appears as a sound rationale for the less positive oxidation potential value observed upon replacing the dihexyloxynaphthalene system by the less sterically demanding dihexhyloxybenzene analogue.

Similar trends were noted for the irreversible oxidation processes in the corresponding dyads. However, the potential values are slightly anodically shifted relative to the parent, unsubstituted oligomers. From this shift, we conclude that small, but notable, electronic interactions prevail between the donating π-conjugated system and the electron acceptor C$_{60}$.

Photophysical Properties. Oligomer References. Oligomer references **4**, **9**, **15**, and **20b** are all strong fluorophores (Figure S2 and Table S1, Supporting Information), which renders them convenient probes for the photophysical measurements with fullerene-containing dyads (**1a**–**d**).

The singlet excited states of **4**, **9**, **15**, and **20b** display, besides their strong emissive features in the 400–550 nm range, characteristic singlet–singlet transitions in the far-visible/near-infrared (Table S1, Supporting Information). For example, photoexcitation of **9** led to the instantaneous formation of a strong maximum in the 800–900 nm region (Figure 1; 20 ps time delay). We ascribe this to the singlet excited-state absorption features of the conjugated π-system. Typically, these transients are short-lived with decay dynamics that obey a monoexponential rate law and rates on the order of 10^9 s^{-1} (Table S1, Supporting Information). While the absorption changes in the near-infrared region (800–900

(28) (a) Döttinger, S. E.; Hohloch, M.; Segura, J. L.; Steinhuber, E.; Hanack, M.; Tompert, A.; Oelkrug, D. *Adv. Mater.* **1997**, *9*, 233. (b) Hohloch, M.; Segura, J. L.; Döttinger, S. E.; Hohnholz, D.; Steinhuber, E.; Spreitzer, H.; Hanack, M. *Synth. Met.* **1997**, *84*, 319.
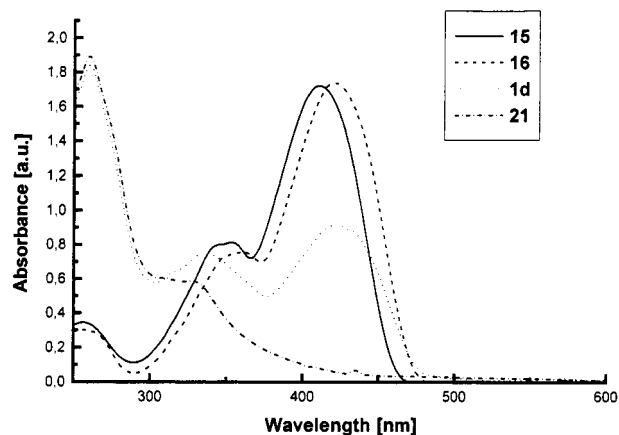

Figure 2. UV–vis spectra of dyad **1d** along with references **15**, **16**, and **21** measured in dichloromethane.

nm) are governed by the disappearance of the singlet–singlet absorption, the simultaneous formation of new maxima was noted in the blue region (Figure 1; 5000 ps time delay). Particularly important is that the time constant of the near-infrared-decay (**9**: 6.0×10^8 s^{-1}) is identical with that of the visible-growth (**9**: 5.7×10^8 s^{-1}). From this, we conclude that a spin-forbidden intersystem crossing (ISC) to the energetically lower-lying triplet excited-state prevails.[29]

Dyads. Steady-State Techniques. Absorption Spectra. The absorption spectra of dyads **1a**–**d** in dichloromethane solutions reveal significant deviations from a simple superposition of the spectra of the individual chromophores (i.e., C$_{60}$ and the conjugated π-systems). As a representative example, the UV–vis spectrum of dyad **1d** is shown in Figure 2, together with that of references **15**, **16**, and **21**. Unequivocally, the maximum observed at 412 nm (**15**) differs from those of **1d** (422 nm) and **16** (420 nm). A similar lack of superimposition was found in toluene, THF and benzonitrile solutions. This further supports the notion (i.e., see electrochemistry) that electronic perturbation exists between the individual chromophores in their ground-state configuration.

Emission Spectra. To shed light on the extent of the electronic interaction between the conjugated π-systems and the fullerene fragment in the excited state, emission measurements were carried out with dyads **1a**–**d** in solvents of different polarity and compared to those of model compounds **4**, **9**, **15**, and **20b**.

In general, the strong emission of the reference compounds (i.e., between 54% and 72%) is quenched in all dyads investigated with values usually between 0.03% and 0.5% (Table 2). It is important to note that, despite the weak fluorescence, the emission patterns of the conjugated π-systems remain unchanged and are not impacted noticeably by the presence of the attached fullerene cores.

By inspecting the fluorescence data in depth a number of important trends can be appreciated, which shall be

(29) The spectral features of the one-electron oxidized products were characterized by pulse radiolytically oxidation experiments. This technique was chosen since it is known to be one of the most powerful tools to investigate reactive intermediates, evolving from the selective one-electron transfer, for example, to [CH$_2$Cl$_2$]$^{\bullet +}$ and $^{\bullet}$OOCH$_2$Cl/$^{\bullet}$-OOCHCl$_2$ peroxyl radicals in oxygenated dichloromethane solutions. Under aerobic conditions, pulse radiolysis of the tested references led to differential absorption spectra, which are characterized by new maxima in the 600–700 nm region.

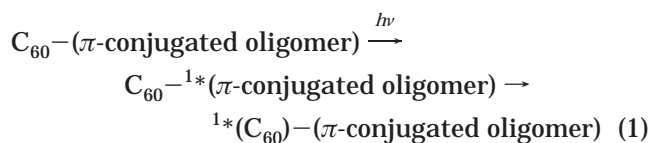**Table 2. Photophysical Data of Fullerene-Based Dyads 1**

compd	21	1a	1b	1c	1d
fluorescence maxima (nm)	715^a 715^b	715^a 715^b	715^a 715^b	715^a 715^b	715^a 715^b
$\Phi_{fluoresc}$ oligomer (toluene)		5.4×10^{-3} ^{c}	2.7×10^{-3} ^{d}	7.6×10^{-4} ^{d}	5.4×10^{-4} ^{d}
$\Phi_{fluoresc}$ oligomer (THF)		4.4×10^{-3} ^{c}	4.1×10^{-3} ^{d}	5.6×10^{-4} ^{d}	3.6×10^{-4} ^{d}
$\Phi_{fluoresc}$ fullerene (toluene)	6.0×10^{-4}	4.98×10^{-4}	4.68×10^{-4} ^{d}	6.0×10^{-4}	6.0×10^{-4} ^{d}
$\Phi_{fluoresc}$ fullerene (THF)	6.0×10^{-4}	4.59×10^{-4}	3.56×10^{-4} ^{d}	2.9×10^{-4}	0.31×10^{-4} ^{d}
k_{energy} (s^{-1}) (toluene)		e	2.9×10^{11}	5.4×10^{11}	5.4×10^{11}
ISC (toluene)	1.35 ns	1.2 ns	1.21 ns	1.22 ns	1.24 ns
ISC (BZCN)	1.39 ns	1.2 ns	1.21 ns	1.29 ns	
$\tau_{fluoresc}$ fullerene (BZCN)	1.38 ns	1.32 ns	1.21 ns	1.39 ns	0.98 ns
triplet maxima (nm)	700	700	700	700	700
$\Phi_{triplet}$ fullerene (toluene)	0.98	0.83	0.64	0.98	0.98
$\Phi_{triplet}$ fullerene (THF)	0.95	0.75	0.59	0.45	radical pair
$\Phi_{triplet}$ fullerene (BZCN)	0.95	0.72	0.57	0.33	radical pair

^{a} In toluene. ^{b} In THF. ^{c} Excitation wavelength 334 nm. ^{d} Excitation wavelength 410 nm. ^{e} No reference available.

discussed in the following. Even in nonpolar toluene the oligomer emission in dyads **1a**−**d** is quenched by up to *3 orders of magnitude*. Instead, the familiar fullerene fluorescence spectrum appears in the near-infrared with a strong *0−0 emission at 715 nm,[30] despite almost exclusive excitation of the oligomer moiety at 410 nm (see Figure 3a). For example, the absorption ratio at 410 nm between the fullerene and oligomer moieties in dyads **1c** and **1d** are 1.5/8.5 and 0.7/9.3, respectively, based on the absorbancies of the components at 410 nm.[31,32]

To unravel, and likewise to test, the mechanism of producing the fullerene emission, a decisive excitation spectrum of the 715 nm emission was taken. In fact, the excitation spectra of dyads **1a**−**d** were reasonable matches of those recorded for the reference models. An illustration

is given in Figure 4, displaying the spectra of trimer **4** and dyad **1b** in different solvents. It should be noted that the maxima further resemble the ground-state transitions. Taking this evidence into account we reach the conclusion that the origin of excited-state energy is that of the conjugated π-systems. Furthermore, it allows to attribute the underlying mechanism: An efficient intramolecular transfer of singlet excited state energy from the photoexcited oligomer to the covalently linked fullerene governs the photophysics of the C_{60}-based arrays.

$$C_{60}-(\pi\text{-conjugated oligomer}) \xrightarrow{h\nu}$$
$$C_{60}-{}^1{}^*(\pi\text{-conjugated oligomer}) \rightarrow$$
$${}^1{}^*(C_{60})-(\pi\text{-conjugated oligomer}) \quad (1)$$

From the quantum yields (Φ) of the fluorescence and the lifetime (τ) of photoexcited **4**, **9**, **15**, and **20b** (**X**), the rate constant (k) for the intramolecular singlet−singlet energy transfer in the investigated dyads (**Y**) can be calculated according to the following expression:

$$k = [\Phi(\mathbf{X}) - \Phi(\mathbf{Y})]/[\tau(\mathbf{X})\,\Phi(\mathbf{Y})] \quad (2)$$

The rate constants are listed in Table 3.[33] Remarkably, the extremely fast rates (10^{11}−10^{12} s^{-1}), as they were

(30) On a different note, it should be considered that, at least, in THF and benzonitrile the fullerene singlet excited state is still powerful enough to guarantee activation of an intramolecular electron-transfer event. Thus, a scenario, in which the singlet−singlet transfer, as it dominates the deactivation in toluene, is followed by an intramolecular electron transfer evolving from the fullerene singlet excited state can principally not be ruled out. It remains, however, questionable at this point, if a 95% emission quenching, as observed in the 1,4-dihexyloxy-benzene/thiophene based dyad and triad, is an accord with the small $-\Delta G_{CS}°$ value (+0.14 in THF and +0.27 in benzonitrile).

(31) Conclusive evidence for the fullerene emission came from experiments that make use of the heavy ion effect for a controlled acceleration of the ISC process between the fullerene singlet and triplet excited states. Addition of ethyl iodide, a heavy atom provider, led to a complete cancellation of this fullerene fluorescence and, instead, the characteristic 824 nm fullerene phosphorescence was detected.[32]

(32) (a) Zeng, Y.; Biczok, L.; Linschitz, H. *J. Phys. Chem.* **1992**, *96*, 5237. (b) Guldi, D. M.; Asmus, K.-D. *J. Phys. Chem. A* **1997**, *101*, 1472. (c) Guldi, D. M.; Maggini, M. *Gaz. Chim. Ital.* **1997**, *127*, 779.

(33) In this context, we like to emphasize that our previously reported values are considered to be too small, a fact that stems from the time resolution of our picosecond apparatus. The latter allowed us only to detect the final fraction of the energy transfer event.
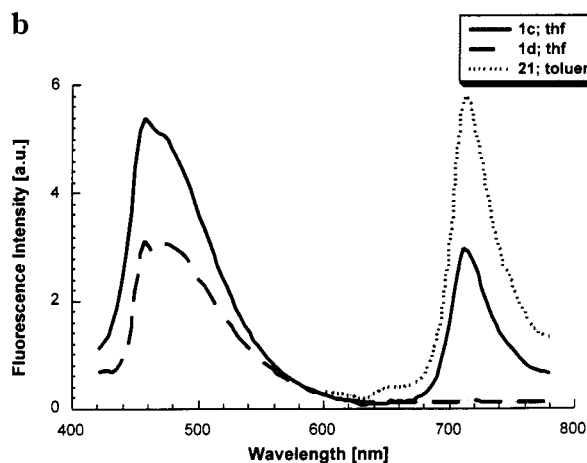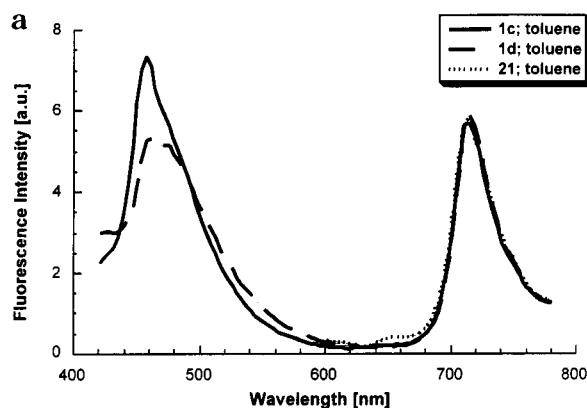
a

b

Figure 3. Emission spectra of dyads **1c** and **1d** in toluene (a) and THF (b) with matching absorption at the 410 nm excitation wavelength (i.e., OD$_{410nm}$ = 0.5).
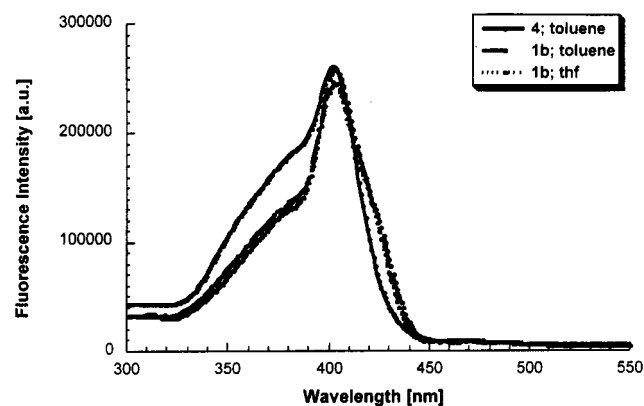

Figure 4. Excitation spectra (normalized to exhibit matching signals around 400 nm) of dyad **1b** in toluene (dotted line) and THF (solid line) and reference **4** in toluene (solid line), monitoring the fullerene emission at 715 nm and oligomer emission at 450 nm, respectively.

determined via this relation, infer a strong coupling between the two moieties, a hypothesis that appears reasonable bearing in mind the appreciable perturbation seen in the ground-state absorption features (vide supra).

By employing reference **21** as a standard, with matching absorption at the excitation wavelength, the fullerene fluorescence quantum yields were deduced for the different donor−acceptor ensembles. In toluene, Φ values nearly approach that measured for the reference **21**, namely, 6.0×10^{-4}, and confirm the efficient transfer of singlet excited-state energy.

Table 3. Driving Force Dependence ($-\Delta G_{CR}°$; $-\Delta G_{CS}°$) and Thermodynamic Parameters (λ; $\Delta G_{CS}^{\ddagger}$) for Intramolecular Electron-Transfer Events in Fullerene-Based Dyads 1

compd	1a	1b	1c	1d
radius donor; R_+ (Å)	2.45	11.35	8.5	7.5
donor−acceptor separation; $R_{D−A}$ (Å)	8.2	16.0	12.8	11.1
$-\Delta G_{CR}°$ [a] (toluene) (eV)	2.89	2.46	2.29	2.02
$-\Delta G_{CR}°$ [a] (THF) (eV)	2.03	2.04	1.86	1.62
$-\Delta G_{CR}°$ [a] (BZCN) (eV)	1.75	1.90	1.74	1.49
$-\Delta G_{CS}°$ [b] (toluene) (eV) oligomer	0.65	0.43	0.62	0.68
$-\Delta G_{CS}°$ [b] (THF) (eV)	1.51	0.85	1.05	1.08
$-\Delta G_{CS}°$ [b] (BZCN) (eV)	1.79	0.99	1.17	1.21
$-\Delta G_{CS}°$ [b] (toluene) (eV) fullerene	−1.13	−0.70	−0.53	−0.26
$-\Delta G_{CS}°$ [b] (THF) (eV)	−0.27	−0.28	−0.10	0.14
$-\Delta G_{CS}°$ [b] (BZCN) (eV)	0.01	−0.14	0.02	0.27
λ [c] (toluene) (eV)	0.39	0.34	0.34	0.34
λ [c] (THF) (eV)	1.43	0.85	0.85	0.82
λ [c] (BZCN) (eV)	1.47	0.87	0.86	0.84
$\Delta G_{CS}^{\ddagger}$ [d] (toluene) (eV) oligomer	0.046	0.006	0.06	0.09
$\Delta G_{CS}^{\ddagger}$ [d] (THF) [eV]	0.001	0	0.012	0.03
$\Delta G_{CS}^{\ddagger}$ [d] (BZCN) (eV)	0.017	0.004	0.027	0.05
$\Delta G_{CS}^{\ddagger}$ [d] (THF) (eV) fullerene				0.14
$\Delta G_{CS}^{\ddagger}$ [d] (BZCN) (eV)			0.21	0.09

[a] Determined from the following relations:

$$-\Delta G_{CR}° = E_{1/2}(D^{\bullet+}/D) - E_{1/2}(A/A^{\bullet-}) + \Delta G_S$$

$$\Delta G_S = \frac{e^2}{4\pi\epsilon_0}\left[\left(\frac{1}{2R_+} + \frac{1}{2R_-} - \frac{1}{R_{D−A}}\right)\frac{1}{\epsilon_S} - \left(\frac{1}{2R_+} + \frac{1}{2R_-}\right)\frac{1}{\epsilon_R}\right]$$

$E_{1/2}(D^{\bullet+}/D)$ = oxidation potential of donor (see Table 1)

$E_{1/2}(A/A^{\bullet-})$ = reduction potential of acceptor (see Table 1)

R_+ = radius donor (see the top of this table)

$R_{D−A}$ = donor−acceptor separation (see the top of this table)

R_- = radius acceptor (4.4 Å)

ϵ_S = solvent dielectric constant (toluene = 2.39; THF = 7.6; benzonitrile = 24.8)

ϵ_R = solvent dielectric constant for electrochemical measurements (9.412)

[b] Determined from the following relation:

$$-\Delta G_{CS}° = \Delta E_{0−0} - (-\Delta G_{CR})$$

$\Delta E_{0−0}$ = excited-state energy of the chromophore

[c] Determined from the following relations:

$$\lambda = \lambda_i + \lambda_S$$

$$\lambda_S = \frac{e^2}{4\pi\epsilon_0}\left[\left(\frac{1}{2R_+} + \frac{1}{2R_-} - \frac{1}{R_{D−A}}\right)\left(\frac{1}{n^2} + \frac{1}{\epsilon_S}\right)\right]$$

λ_i = internal reorganization energy (0.3 eV)

λ_S = solvent reorganization energy

n = solvent refractive index (toluene = 1.496; THF = 1.407; benzonitrile = 1.528)

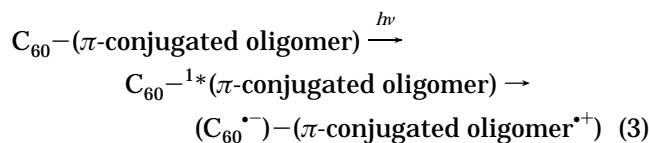[d] determined from the following relation:

$$\Delta G_{CS}^{\ddagger} = \frac{(\Delta G_{CS} + \lambda)^2}{4\lambda}$$

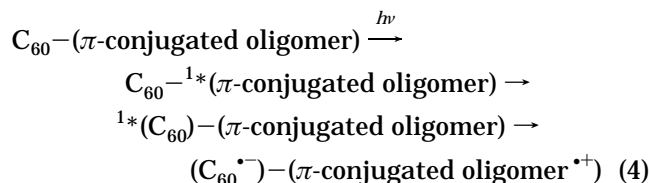$\Delta G^{\ddagger}$ = Gibbs activation energy

Next, we shift the focus to a more polar solvent (i.e., THF). To facilitate the discussion and interpretation, we

group dyads **1a**–**d** into two different categories. The first class comprises the dihexyloxynaphthalene system (**20**, **1a**) and its trimeric analogue (**4**, **1b**), both displaying high oxidation potentials, while the lower potentials of dihexyloxynaphthalene−thiophene (**9**, **1c**) and dihexyloxybenzene−thiophene (**15**, **1d**) lead us to deal with them separately.

Similar to the trends seen for toluene, the emission of the conjugated π-system in dyads **1a**–**d** in THF is strongly quenched compared to the emission of the corresponding references, with quantum yields that are somewhat smaller than in toluene. By contrast, the fullerene fluorescence quantum yields deviate substantially from this tendency (see Figure 3b). Considering the quantum yields in the first group, the THF values diverge moderately by ∼10% and ∼22% from the corresponding toluene values for the monomeric (**1a**) and trimeric dihexyloxynaphthalene (**1b**), respectively. Substantial effects were, however, seen in the second category. In particular, the differences between the toluene and THF samples were 57% (dihexyloxynaphthalene−thiophene, **1c**) and 95% (dihexyloxybenzene−thiophene, **1d**). These values testify to the presence of yet another second pathway, competing with the energy transfer in the overall deactivation of the photoexcited chromophore. At first glance, a highly exothermic electron-transfer scenario could be considered as a conceivable rationale for the absence of the fullerene emission.

$$C_{60}-(\pi\text{-conjugated oligomer}) \xrightarrow{h\nu}$$
$$C_{60}-{}^{1}*(\pi\text{-conjugated oligomer}) \rightarrow$$
$$(C_{60}{}^{\bullet-})-(\pi\text{-conjugated oligomer}{}^{\bullet+}) \quad (3)$$

Another plausible alternative implies the following sequential energy and electron-transfer events:

$$C_{60}-(\pi\text{-conjugated oligomer}) \xrightarrow{h\nu}$$
$$C_{60}-{}^{1}*(\pi\text{-conjugated oligomer}) \rightarrow$$
$${}^{1}*(C_{60})-(\pi\text{-conjugated oligomer}) \rightarrow$$
$$(C_{60}{}^{\bullet-})-(\pi\text{-conjugated oligomer}{}^{\bullet+}) \quad (4)$$

Thermodynamic Considerations. Looking at the emission quenching and, more importantly, at the varying donor strength of **4**, **9**, **15**, and **20b**, we gathered that an intramolecular electron transfer, evolving from the excited chromophore to the fullerene moiety, may compete with an energy transfer. As a test to validate the above conclusion, the driving forces ($-\Delta G_{CS}°$), associated with an intramolecular charge separation, were calculated in accordance with the approximations given in Table 3.[34]

The model gives rise to large $-\Delta G_{CS}°$ values in toluene, THF, and benzonitrile (Table 3) for **1a**–**c**. Considering, however, the energy of the fullerene singlet excited state of 1.76 eV, relative to those of the charge-separated state, it is clear that the largest energy gap opens between the two singlet excited states (i.e., oligomer and fullerene). Consequently, the energy-transfer route is the thermodynamically favored pathway. From this we can assume that after the completion of the singlet−singlet energy transfer the fullerene singlet excited state can only decay
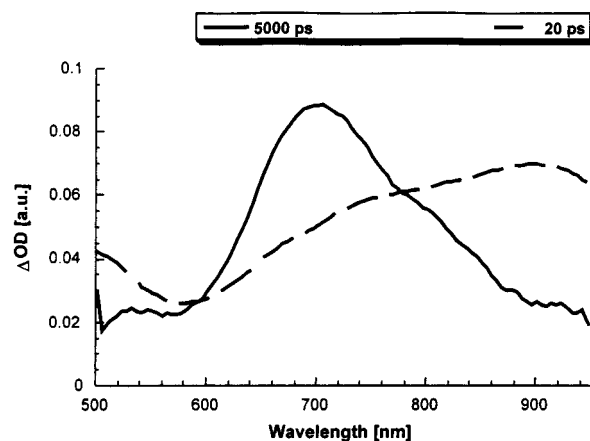
(34) Atkins, P. W.; MacDermott, A. J. *J. Chem. Educ.* **1982**, *59*, 359.

Figure 5. Transient absorption spectrum (visible-near-infrared part) recorded 20 ps (dashed line) and 5000 ps (solid line) upon flash photolysis of dyad **1d** (∼5.0 × 10⁻⁵ M) at 355 nm in deoxygenated toluene, indicating the fullerene singlet−singlet ($\lambda_{max} = 900$ nm) and triplet−triplet features ($\lambda_{max} = 700$ nm), respectively.

to the triplet excited state and finally to the singlet ground state.

The picture is quite different for the dihexyloxybenzene−thiophene-based dyad (**1d**). In fact, the moderate oxidation potential of the dihexyloxybenzene-thiophene donor shifts the energy of the charge-separated state in both THF and benzonitrile markedly below that of the fullerene singlet excited state. Hence, it is likely that charge separation plays the dominant role, an assumption, which is consistent with the fluorescence data. The latter showed a complete abolishment of the fullerene fluorescence in THF and benzonitrile (Table 3). The energy levels, as extracted from Tables 1 and 3, are shown in Scheme S1a (toluene) and S1b (benzonitrile) (Supporting Information) to illustrate the different relaxation pathways of the photoexcited states.

Time-Resolved Techniques. The conclusion of the emission studies along with the thermodynamic calculations presumes that an intramolecular electron-transfer scenario competes with an intramolecular energy transfer led us to characterize the fullerene-based hybrids by time-resolved transient absorption spectroscopy in different solvents.

Transient Spectroscopy in Nonpolar Toluene. In nonpolar toluene, the fluorescence experiments reveal the same reactivity for all dyads, which led us to exemplify the transient features by describing dyad **1d** in detail.

Transient absorption changes, recorded upon 18 ps laser excitation of the investigated dyads, are superimposable with those recorded for the fullerene model (**21**), despite the predominant excitation of the conjugated π-systems. The absorption ratio—fullerene versus oligomer—at 355 nm in dyad **1d** is, for example 3.3/6.7. In Figure 5 the differential changes for **1d** are shown after a 20 ps time delay. Instead of the singlet−singlet absorption of the oligomer units (see for illustration Figure 1), broad maxima, which correspond to the fullerene singlet−singlet absorption, were found around 900 nm. Similar spectra were noted for dyads **1a**–**c** in toluene.

Time profiles, taken at various wavelengths, indicate that the singlet excited state is formed instantaneously and in a single step. The formation dynamics are masked
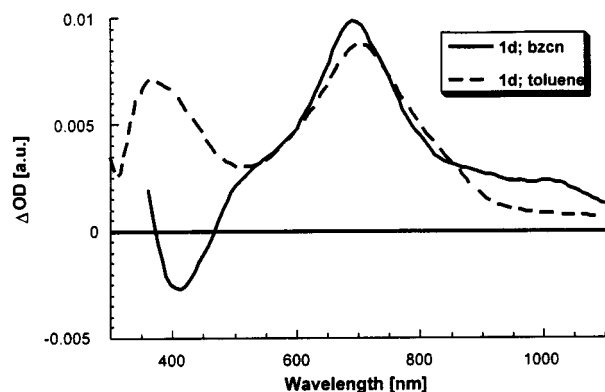
Figure 6. Transient absorption spectrum (visible-near-infrared part) recorded 50 ns upon flash photolysis of dyad **1d** (2.0 × 10^{-5} M) at 355 nm in deoxygenated toluene (dashed line) and deoxygenated benzonitrile solutions (solid line), indicating the fullerene triplet−triplet (λ_{max} at 360 and 700 nm) and the charge-separated radical pair features (λ_{max} at 680 and 1000 nm), respectively.

Figure 7. Transient absorption spectrum (visible-near-infrared part) recorded 20 ps upon flash photolysis of dyad **1c** (dashed line) and **1d** (solid line) (2.0 × 10^{-5} M) at 355 nm in deoxygenated benzonitrile, indicating the oligomer π-radical cation features (λ_{max} around 700).

by the apparatus's resolution (18 ps). This allowed only estimation of the intramolecular rate constant for the energy transfer process ($k \geq 5.0 \times 10^{10}$ s^{-1}), which appears credible in light of the rates derived from the fluorescence data. Hereafter, an ISC is the predominant deactivation of the fullerene singlet excited states. The accordingly formed triplet excited state reveal characteristic peaks around 700 nm (Figure 5; 5000 ps time delay).

In line with the proposed energy-transfer mechanism (eq 1), the differential absorption changes, recorded immediately after an 8 ns pulse (Figure 6), showed the same spectral features of the fullerene triplet excited state as observed at the end of the picosecond experiments. Precisely, two maxima located at 360 and 700 nm and a low-energy shoulder around 800 nm were observed. Thus, our analysis clearly shows the photosensitization effect of the conjugated π-system chromophore, acting as an antenna system and transmitting its excited energy to the covalently attached fullerene moieties. The overall triplet quantum yields (Table 2), as measured with the comparative method (i.e., using **21** as a standard), in toluene vary between 0.64 and 0.98 and are slightly lower than the one found for the reference compound ($\Phi_{triplet} = 0.98$).

Transient Spectroscopy in Polar Benzonitrile. The choice of this strongly polar solvent led to a different reactivity. In particular, the dihexyloxybenzene−thiophene-based dyad (**1d**) gave rise, following the 18 ps laser pulse, to the immediate occurrence of a 690 nm band, as shown in Figure 7. In accordance with the pulse radiolytic oxidation experiments, we assign this transient absorption to the π-radical cation of the oligomer. The fast grow-in ($\leq$18 ps) supports the direct mechanism (eq 3), rather than the sequential mechanism (eq 4). This reactivity reflects the emission studies (vide supra), implying that the energy of the charge-separated state (1.49 eV) is below that of the fullerene singlet excited state.

Raising the oxidation potential (i.e., dihexyloxynaphthalene−thiophene; **1c**) and, in turn, bringing the energy of the charge-separated state (1.74 eV) close to that of the fullerene singlet led to the detection of two photoproducts. This is illustrated in Figure 7, which displays the transient absorption changes recorded immediately
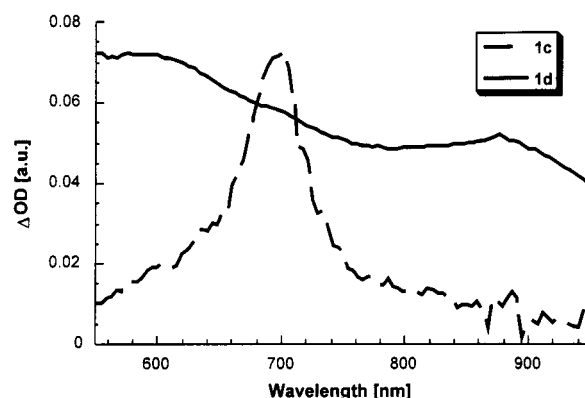
(20 ps) after irradiating **1c** with a picosecond laser pulse. Charge separation was inferred on the basis of the instantaneously produced 700 nm maximum, while the presence of the 900 nm absorption and an ISC rate of 7.1 × 10^8 s^{-1} are clear attributes connected with the energy transfer product.

In sharp contrast to the dihexyloxybenzene−thiophene (**1d**) and dihexyloxynaphthalene−thiophene (**1c**) systems are the picosecond changes of **1b** and **1a**. They are overshadowed by the dominance of the fullerene photophysics (similar to Figure 5), namely, instantaneous formation of the singlet excited state followed by the subsequent ISC. A plausible explanation for this observation is the unfavorably raised energies of the charge-separated state (1.90 eV), which in the dihexyloxynaphthalene systems even passed that of the fullerene singlet (Table 3).

Full spectral characterization of the charge-separated state was accomplished directly with the help of complementary nanosecond measurements. For example, photolysis of a benzonitrile solution of **1d** led to maxima at 1000 and 680 nm (Figure 6). Based on a spectral comparison, we ascribe the former band to the fullerene π-radical anion, while the latter reveals the broad characteristics of the dihexyloxybenzene-thiophene π-radical cation. In accordance with these results, we propose the occurrence of a photoinduced electron transfer, evolving from the singlet excited state of the chromophore (i.e., conjugated π-system) to the electron-accepting fullerene (eq 3).

More complicated is the situation encountered upon raising the oxidation potential of the donor, especially in the dihexyloxynaphthalene-based donor−acceptor ensembles. In these cases, the strong triplet−triplet absorption (ϵ_{700nm} ~16 100 M^{-1} cm^{-1}) dominates both the pico- and nanosecond spectra. Consequently, to obtain direct evidence in support of the weaker absorbing radical pair (ϵ_{1000nm} ~8000 M^{-1} cm^{-1}) in **1a** and **1b**, subtraction of the triplet absorption features from, for example, the nanosecond spectrum became necessary. The resulting differential absorption changes reveal a near-infrared maximum at 1000 nm and a visible-doublet at 660 and 800 nm, which are characteristics of the reduced fullerene moiety and the oxidized dihexyloxynaphthalene system **4** (see above), respectively.[35]
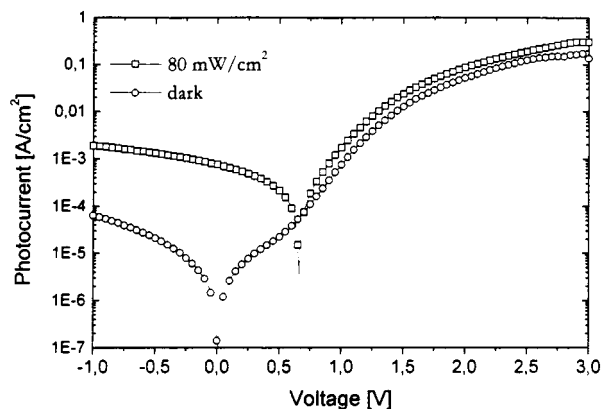
Figure 8. I/V characteristics of a ITO/PEDOT/**1d**/LiF/al diode under 80 mW/cm² white light (open squares) from a solar simulator and in the dark (open circles).

Figure 9. Spectrally resolved photocurrent, converted to incident photon to converted electron efficiency (IPCE) of photodiodes from **1d**.

Both fingerprints allowed us to determine the lifetime of the associated charge-separated state. The decay curves were well fitted by a single-exponential decay component. In particular, lifetimes that are on the order of a microsecond were derived from the decays of the oxidized donor and reduced acceptor absorption at 680 and 1000 nm, respectively (see Figure S3, Supporting Information). Additional proof for an intramolecular charge recombination stems from a set of experiments, conducted with different laser power and different dyad concentrations. In particular, decreasing the radical-pair concentration in various increments by up to 65% led to a maximal change of the radical pair lifetime. In other words, a contribution, stemming from an intermolecular charge recombination process, is assumed to be insignificant. In general, the lifetimes of the charge-separated states can be correlated with the solvent polarity. In the case of **1d** (0.71 μs (THF), 1.37 μs (benzonitrile)) the lifetimes clearly increase as the solvent polarity increases.

Devices. Since an optimized electron transfer is an imperative requisite for devising a high-performance photovoltaic device, we probed the photovoltaic properties of dyad **1d**, which in solution shows an all-electron-transfer behavior when sandwiched between asymmetric electrodes and forming a quasi ohmic contact. In principle, this approach gives rise to a structure similar to that of metal−insulator−metal (MIM) diodes. Devices that are based on such an electrode configuration are expected to lead to an asymmetric current-to-voltage behavior, independent of the rectifying properties of the molecule. A reverse bias direction (i.e., electron injection into the oligomer and hole injection into the fullerene), for example, for **1d** is energetically unfavorable. Conversely, a forward bias resulting in an electron injection into the fullerene and hole injection into the oligomer is energetically favorable.

Typical current-to-voltage characteristics of **1d**, under illumination and also in the dark, are given in Figure 8. The dark I/V curve is symmetric in the region between +0.5 and −0.5 V, which is, in part, due to a small shunt resistivity of the diode leading to an ohmic contribution. A diode turn on behavior is observed at voltages higher than 0.7 V, with rectification ratios of more than 2 orders
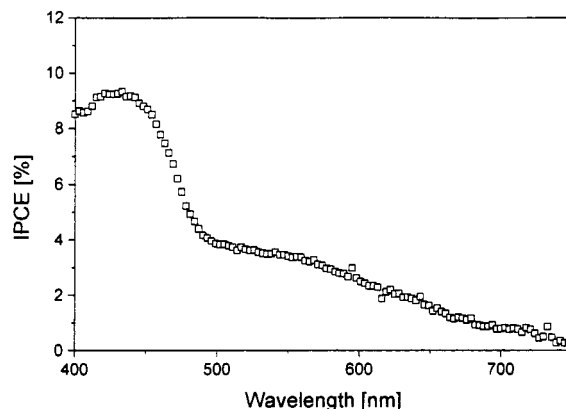
in magnitude. The high quality of the diode further confirms that **1d** exhibits sufficiently good film forming properties when processed from solution. This allows to cast thin films with a closed surface. Under irradiation with AM 1.5 solar simulated light with 80 mW/cm², an open circuit voltage of 0.67 V, a short circuit current of 0.75 mA/cm², and a fill factor <0.3 were measured. Taken all these parameters into concert, we conclude an overall white light power efficiency of ≤0.2%.

In addition, the results stemming from the spectral photocurrent measurements (Figure 9) are encouraging. A monochromatic peak efficiency of ∼10% (IPCE) was measured at 440 nm, directly proving the contribution of the oligomer (see Figure 6) to the photocurrent. Between 500 and 700 nm, the IPCE drops below 4%. In this energy region the photocurrent generation is, however, due to a photoinduced hole transfer of the weakly absorbing fullerene to the covalently linked oligomer unit.

Summary

The synthesis of fulleropyrrolidines, covalently linked to fluorescent π-conjugated systems bearing long alkyl chains, has been carried out from suitably functionalized oligomers by 1,3-dipolar cycloaddition reaction of azomethine ylides to C_{60}.

Cyclic voltammetry reveals the presence of three one-electron reduction steps, occurring all at the fullerene electron acceptor. On the anodic side, only a single one-electron oxidation wave is observed, which relates to the oxidation of the oligomeric unit. This oxidation wave is shifted to less positive values when replacing the peripheral naphthalene units in the trimeric system (**1b**) by thiophene rings (**1c**). Additionally, substitution of the central naphthalene unit by a phenylene moiety (**1d**) further increases the electron donor ability.

By controlling the structure of fluorescent π-conjugated systems, the outcome of an ultra rapid intramolecular deactivation of a photoexcited oligomer core was successfully shifted from an all energy transfer to an all electron-transfer scenario. In particular, the different oxidation potentials of, for example, dihexyloxynaphthalene (i.e., monomeric and trimeric form), dihexyloxybenzene/thiophene and dihexyloxynaphthalene/thiophene moieties helped to direct the competition between these two transfer channels. Hereby, the relative position of the charge-separated state in reference to the fullerene

---

(35) This subtraction procedure hampered a meaningful analysis of the charge recombination kinetics.

singlet excited state determines the nature of the photoproduct: Only the energetically lowest lying state is populated in high yields.

Photovoltaic devices confirm the efficient photoinduced charge generation within one of the investigated donor–acceptor ensembles (**1d**). Spectrally resolved photocurrent measurements revealed contributions from both the oligomer and the fullerene moiety to the photocurrent generation. Moreover, photovoltaic devices showed white light efficiencies up to ~0.2%. This is one of the highest values ever reported for a solution processed single component organic solar cell. In fact, charge generation, as well as electrical current rectification, may indeed be cooperatively realized within this molecular donor–acceptor ensemble, thereby combining both essential features for photovoltaics within a single molecule.

Currently, we are directing our efforts toward optimizing parameters such as the thickness and morphology of the active layer, which are expected to lead to further improved and higher photocurrent efficiencies.

Experimental Section

Picosecond laser flash photolysis experiments were carried out with 355-nm laser pulses from a mode-locked laser system (pulse width 18 ps, 2–3 mJ/pulse). The white continuum picosecond probe pulse was generated by passing the fundamental output through a D$_2$O/H$_2$O solution. The excitation and the probe were fed to a spectrograph with fiberoptic cables and were analyzed with a dual diode array detector interfaced with a computer. The nanosecond laser flash photolysis were performed with laser pulses from a nitrogen laser system (337.1 nm, 8 ns pulse width, 1 mJ/pulse). A typical experiment consisted of 5–10 replicate pulses per measurement.

Fluorescence lifetimes were measured with a laser strope fluorescence lifetime spectrometer with 337 nm laser pulses from a nitrogen laser fiber coupled to a lens-based T-formal sample compartment equipped with a stroboscopic detector. Fluorescence spectra were measured in methylcyclohexane solutions containing fullerene forming clear, noncracking glasses in liquid nitrogen. In the case of any other solvents, the experiments were performed at room temperature. A 570 nm long-pass filter in the emission path was used in order to eliminate the interference from the solvent and stray light for recording the fullerene fluorescence. No corrections were performed for the fluorescence, but long integration times (20 s) and low increments (0.1 nm) were applied. The slits were 2 and 8 nm, and each spectrum was an average of at least five individual scans.

Devices were fabricated by spin coating **1d** from a 1.2% toluene/chlorobenzene (3:2) solution until a thickness of approximately 60 nm on top of an ITO/PEDOT:PSS substrate was achieved. A LiF/Al (6 Å/100 nm) layer was thermally deposited as a top electrode in a two-step evaporation process through a shadow mask to define a device area of 3.3 mm^2. Thus, the insertion of the LiF layer ensures better contacts with low contact resistivities.[36,37]

Cyclic voltammograms were recorded on a potentiostat/galvanostat in a conventional three-compartment cell equipped with a software electrochemical analysis by using a GCE (glassy carbon) as working electrode, SCE as reference electrode, Bu$_4$NClO$_4$ as supporting electrolyte, a toluene–acetonitrile solvent mixture (v/v 4:1), and at a scan rate of 200 mV/s. All melting points were measured with a melting point apparatus and are uncorrected.

FTIR spectra were recorded either as KBr pellets. ^{13}C and ^{1}H NMR spectra were recorded with a 300 MHz for ^{1}H and 75

(36) Jabbour, G. E.; Kippelen, B.; Armstrong, N. R.; Peyghambarian, N. *Appl. Phys. Lett.* **1998**, *73*, 1185.

(37) Hung, L. S.; Tang, C. W.; Mason, M. G. *Appl. Phys. Lett.* **1997**, *70*, 152.

MHz for ^{13}C spectrometer. Chemical shifts are given as δ values (internal standard: TMS). 2-Bromo-5-formylthiophene (**8b**), 2-formylthiophene (**8a**), 1,5-dihydroxynaphthalene, 1,4-hydroquinone, sarcosine, and [60]fullerene are commercially available and were used without further purification. Some of the functionalized π-conjugated systems (**5**,[20] **10**,[21b] **13**,[21b] and **14**[21a]) and reference compounds (**4**,[20] **20**,[20] and **21**[26]) were obtained by following previously described synthetic procedures. Tetrahydrofuran and dimethylformamide were dried with sodium and calcium hydride, respectively, while chloroform and dichloromethane were distilled from CaCl$_2$.

1,3-Dipolar Cycloaddition Reactions. Synthesis of Dyads. General Procedure. A mixture of 0.05 mmol of monoaldehyde, 38 mg (0.05 mmol) of [60]fullerene, and 0.25 mmol of *N*-methylglycine (sarcosine) was dissolved in 30 mL of toluene, and the mixture was refluxed for 24 h. After this time, the reaction was allowed to reach room temperature, and then the solvent was partially vacuum-evaporated and poured on a silica gel column. The black solid obtained after chromatography (cyclohexane/toluene) was further purified by repetitive centrifugation using methanol and diethyl ether to yield the corresponding dyads as black solids.

***N*-Methyl-2′-(6-bromo-1,5-dihexyloxy-2-naphthyl)pyrrolidino[3′,4′:1,2][60]fullerene (1a).** By following the above general procedure and using monoaldehyde **3b**[28] as the starting material, 16 mg (27%) of dyad **1a** was obtained: ^{1}H NMR (CDCl$_3$, 300 MHz) δ 8.20 (d, 1H, $J = 8.9$ Hz), 7.97 (d, 1H, $J = 8.9$ Hz), 7.71 (d, 1H, $J = 9.0$ Hz), 7.58 (d, 1H, $J = 9.0$ Hz), 5.57 (s, 1H), 5.04 (d, 1H, $J = 9.4$ Hz), 4.32 (d, 1H, $J = 9.4$ Hz), 4.16–4.07 (m, 4H), 2.77 (s, 3H), 2.07–1.90 (m, 4H), 1.58–1.37 (m, 12H), 0.96 (t, 6H); ^{13}C NMR (CDCl$_3$, 75 MHz) δ 156.28, 155.47, 154.33, 154.03, 153.22, 152.75, 147.20, 147.17, 146.50, 146.42, 146.19, 146.11, 146.05, 146.00, 145.96, 145.86, 145.84, 145.61, 145.46, 145.41, 145.29, 145.25, 145.19, 145.11, 145.03, 142.98, 142.90, 142.54, 142.50, 142.45, 142.42, 142.18, 142.16, 142.04, 142.01, 141.91, 141.29, 141.67, 141.62, 141.49, 140.10, 140.02, 139.72, 139.54, 136.78, 136.43, 135.73, 134.85, 130.80, 130.15, 128.79, 127.88, 126.27, 119.74, 118.55, 117.46, 113.83, 77.21, 76.65, 76.37, 76.04, 74.42, 69.92, 31.74, 31.68, 30.41, 30.21, 25.96, 25.64, 22.75, 22.57, 14.17, 14.05; FTIR (KBr, cm^{-1}) 2920, 2850, 2774, 1620, 1581, 1427, 1407, 1361, 1331, 1177, 1024, 526; MS *m/z* (APCI) (rel intensity) 1184 (M$^+$, 100), 1105 (28).

Pyrrolidino[3′,4′:1,2][60]fullerene 1b. By following the above general procedure and using monoaldehyde **7** as the starting material, 58 mg (63%) of dyad **1b** was obtained: ^{1}H NMR (CDCl$_3$, 300 MHz) δ 8.10 (d, 2H, $J = 9.0$ Hz), 7.94 (d, 2H, $J = 8.8$ Hz), 7.97–7.89 (m, 6H), 7.81–7.74 (m, 4H), 7.59 (d, 2H, $J = 8.8$ Hz), 5.54 (s, 1H), 4.98 (d, 1H, $J = 9.6$ Hz), 4.27 (d, 1H, $J = 9.6$ Hz), 4.19–4.14 (m, 2H), 4.10–4.03 (m, 10H), 2.74 (s 3H), 1.98 (t, 12H), 1.59 (s, 12H), 1.35 (s, 24H), 0.88 (t, 18H); ^{13}C NMR (CDCl$_3$, 75 MHz) δ 155.62, 154.59, 154.22, 153.37, 147.27, 146.55, 146.21, 146.09, 145.94, 145.74, 145.55, 145.28, 145.21, 144.56, 144.44, 142.99, 142.59, 142.27, 142.13, 141.78, 141.60, 140.11, 139.83, 139.17, 136.85, 136.56, 135.88, 134.94, 130.44–113.55 (54C), 74.59, 70.06, 69.57, 40.15, 31.86, 31.83, 31.79, 31.75, 30.55, 30.30, 26.14, 26.10, 25.76, 22.86, 22.74, 22.66, 14.26, 14.08; FTIR (KBr, cm^{-1}) 2922, 2853, 1462, 1406, 1340, 1176, 1042, 816, 526; MS *m/z* (ESI) (rel intensity) 1886 (M$^+$ + 23, 100). Anal. Calcd for C$_{133}$H$_{100}$BrNO$_4$: C, 84.60; H, 5.34; N, 0.74. Found: C, 82.36; H, 5.47, N, 0.94.

Pyrrolidino[3′,4′:1,2][60]fullerene (1c). By following the above general procedure and using monoaldehyde **13** as the starting material, 26 mg (39%) of dyad **1c** was obtained: ^{1}H NMR (CDCl$_3$, 300 MHz) δ 7.86 (d, 1H, $J = 9.0$ Hz), 7.84 (d, 1H, $J = 9.0$ Hz), 7.70 (d, 2H, $J = 9.0$ Hz), 7.63 (m, 1H), 7.58 (d, 2H, $J_{trans} = 16.4$ Hz), 7.39–7.33 (m, 1H), 7.26 (d, 2H, $J_{trans} = 16.4$ Hz), 7.07 (d, 2H, $J = 3.9$ Hz), 5.15 (s, 1H), 5.01 (d, 1H, $J = 9.7$ Hz), 4.26 (d, 1H, $J = 9.7$ Hz), 3.99 (t, 4H), 2.86 (s, 3H), 1.86 (q, 4H), 1.31 (m, 12H), 0.85 (t, 6H); ^{13}C NMR (CDCl$_3$, 75 MHz) δ 161.39, 154.19, 153.21, 150.84, 147.35, 147.34, 147.33, 146.75, 146.35, 146.34, 146.23, 146.20, 146.15, 146.12, 145.97, 145.95, 145.79, 145.61, 145.57, 145.49, 145.45, 145.38, 145.32, 145.29, 145.28, 145.19, 144.72, 144.59, 144.36, 144.35, 143.15, 142.98, 142.72, 142.61, 142.59, 142.22, 142.18, 142.17, 142.13,

142.07, 142.06, 141.97, 141.93, 141.91, 141.69, 141.61, 140.19, 139.93, 139.76, 138.12, 135.85, 135.57, 130.17, 129.34, 129.02, 128.21, 127.18, 126.64, 125.45, 124.85, 123.71, 123.09, 122.93, 120.42, 118.99, 118.87, 114.51, 107.09, 77.19, 76.32, 75.98, 68.68, 50.87, 40.39, 31.86, 31.76, 30.44, 30.42, 26.18, 26.06, 22.77, 22.68, 14.24, 14.08; FTIR (KBr, cm^{-1}) 2930, 2864, 2216, 1500, 1440, 1224, 526; MS m/z (ESI) (rel intensity) 1345 (M$^+$ + 1, 100), 685 (40). Anal. Calcd for C$_{98}$H$_{44}$N$_2$O$_2$S$_2$: C, 87.48; H, 3.30; N, 2.08; S, 4.77. Found: C, 85.82; H, 3.93, N, 1.75; S, 4.57.

Pyrrolidino[3′,4′:1,2][60]fullerene (1d). By following the above general procedure and using monoaldehyde **18** as the starting material, 19 mg (27%) of dyad **1d** was obtained: ^{1}H NMR (CDCl$_3$, 300 MHz) δ 7.25 (d, 1H, J = 3.6 Hz), 7.24 (d, 2H, J_{trans} = 16.3 Hz), 7. 04 (d, 2H, J_{trans} = 16.3 Hz), 7.14−7.13 (m, 1H), 7.01−6.97 (m, 2H), 6.94 (d, 1H, J = 3.6 Hz), 6.77 (d, 1H, J = 3.9 Hz), 5.15 (s, 1H), 4.92 (d, 1H, J = 9.6 Hz), 4.18 (d, 1H, J = 9.6 Hz), 3.94 (m, 4H), 2.87 (s, 3H), 1.76 (q, 4H), 1.32 (s, 12H), 0.85 (t, 6H); ^{13}C NMR (CDCl$_3$, 75 MHz) δ 155.84, 153.92, 153.16, 153.14, 151.08, 151.06, 147.33, 146.87, 146.35, 146.32, 146.30, 146.22, 146.18, 146.15, 146.01, 145.96, 145.95, 145.79, 145.58, 145.54, 145.52, 145.46, 145.36, 145.31, 145.27, 145.18, 144.94, 144.71, 144.62, 144.37, 143.16, 142.97, 142.71, 142.60, 142.58, 142.26, 142.21, 142.17, 142.15, 142.08, 142.06,

141.98, 141.95, 141.68, 141.61, 140.17, 139.92, 139.78, 139.58, 137.06, 136.63, 135.85, 135.61, 130.45, 128.73, 126.55, 126.03, 125.79, 125.20, 123.89, 123.70, 122.40, 121.54, 110.89, 110.78, 110.55, 79.57, 77.10, 70.03, 69.49, 68.81, 40.35, 31.57, 29.34, 25.86, 22.62, 14.08; FTIR (KBr, cm^{-1}) 2932, 2860, 2788, 1497, 1461, 1420, 1334, 1202, 960, 526. Anal. Calcd for C$_{93}$H$_{42}$-BrNO$_2$S$_2$: C, 82.78; H, 3.14; N, 1.04; S, 4.75. Found: C, 82.12; H, 3.38, N, 1.02; S, 4.59.

Supporting Information Available: Synthetic Procedures, cyclic voltammograms and some additional photophysical information. This material is available free of charge via the Internet at http://pubs.acs.org.

JO0108313